Electronic Supplementary Material (ESI) for Physical Chemistry Chemical Physics.

Electronic Supplementary Information

Kinetics and pressure-dependent HO_x yields of the reaction between Criegee intermediate CH_2OO and HNO_3

Pei-Ling Luo*[a]

[a]Institute of Atomic and Molecular Sciences, Academia Sinica, Taipei 10617, Taiwan.
*E-mail: plluo@gate.sinica.edu.tw

Table of content

Note S1. Descriptions of adopted kinetic model and reaction rate coefficients.

In kinetic studies, the simplified kinetic model (Table S1) was employed to determine the rate coefficients of the reaction CH_2OO + HNO_3. The simplified kinetic scheme takes into account key reaction paths including the formation and self-reaction of CH_2OO as well as the CH_2OO + I reaction.[1–5] To fit the first-order rate coefficient k^I (= k_7×[HNO_3]$_0$ in Table S1), all rate coefficients at values listed in Table S1 were fixed and the initial concentrations [CH_2I]$_0$, [O_2]$_0$, and [HNO_3]$_0$ were given. The root mean square error (RMSE) of each fitted residual was obtained to be ~3 % under wide variations in experimental conditions, indicating the adequacy of the adopted kinetic model.

To determine the branching ratios for the OH + $CH_2(O)NO_3$ and NO_2 + CH_2O + HO_2 product channels of the reaction CH_2OO + HNO_3, the global kinetic model (Table S4) was used to simulate the temporal concentration profiles of CH_2OO, CH_2O, OH, and HO_2. The global kinetic model has been explored by quantitative analysis of the time traces of CH_2OO, CH_2O, OH and HO_2 radicals recorded under varied experimental conditions with and without the addition of SO_2.[2] The global kinetic scheme takes into account the reaction pathways related to the formation of the OH and HO_2 radicals that could be formed from decomposition of initially energized and vibrationally excited Criegee intermediates. To investigate the reaction CH_2OO + HNO_3, only the pathways of CH_2OO + SO_2 in the previous work were replaced to the pathways of CH_2OO + HNO_3. Additionally, to simplify the model, only three product channels of the reaction CH_2OO + HNO_3 were listed in the model:

$$CH_2OO + HNO_3 \rightarrow OH + CH_2(O)NO_3 \quad (R_{7a})$$
$$CH_2OO + HNO_3 \rightarrow NO_2 + CH_2O + HO_2 \quad (R_{7b})$$
$$CH_2OO + HNO_3 \rightarrow \text{other products} \quad (R_{7c})$$

in which the branching ratios for the OH + $CH_2(O)NO_3$ and NO_2 + CH_2O + HO_2 product channels are y_{OH} and y_{HO2}, respectively, and the branching ratio for other products is $1- y_{OH} - y_{HO2}$. In addition, the rate coefficients of the reaction vibrationally excited $CH_2OO^{\#}$ + HNO_3 ($R_{11a–11c}$) were set as same as that of the reaction CH_2OO + HNO_3 ($R_{7a–7c}$).

In the reaction system, the OH radicals might be reacted away mainly with the precursor CH_2I_2 or the product I_2 and NMHP. Due to lack of the accurate rate coefficients of these reactions, the overall decay rate (k_{18}) of the OH radicals was obtained by fitting the time trace with a single exponential-decay function, as shown in Fig. S4(a). Afterwards, the y_{OH} could be obtained by fitting the time traces using the global kinetic model with the fixed overall decay rate (k_{18}). Considering an uncertainty of 10% on obtained concentrations of the OH radicals, the y_{OH} would be varied by ~20%, as shown in Figs. S4(b).

With the addition of HNO_3, the HO_2 radicals can be quickly generated and followed by a slow decay through the underlying reaction pathways (R_{19}–R_{21}). Because the overall decay rates (10^1~10^2 s^{-1}) are much smaller than the formation rates (10^4~10^5 s^{-1}), the y_{HO2} could be determined by simulating the time traces with the kinetic model excluding the loss pathways of HO_2 (R_{19}–R_{21}). Considering an uncertainty of 10% on obtained concentrations of the HO_2 radicals, the y_{HO2} would be varied by ~10%,

as shown in Figs. S5(a). Afterwards, the additional loss rate (k_{21}) for the HO_2 radicals can be obtained by fitting the measured traces with the global kinetic model and the fixed y_{HO2}, as shown in Fig. S5(b).

In the absence of HNO_3, about 90% CH_2OO would be reacted to form CH_2O via self-reaction of CH_2OO and the reaction CH_2OO + I. In the experiments, the formation rates of CH_2O increase, but the yields of CH_2O decrease with the addition of HNO_3, indicating that a part of CH_2O could be generated from the reaction $CH_2OO + HNO_3$, but the fractional yields of the CH_2O product channel of the reaction $CH_2OO + HNO_3$ might be lower comparing to that of the reactions $CH_2OO + CH_2OO$ and CH_2OO + I. The temporal concentration profile of CH_2O can be also fitted with kinetic model to derive the branching ratio (y_{HO2}) for the $NO_2 + CH_2O + HO_2$ product channel and the derived y_{HO2} is consistent with the value obtained by analyzing the time trace of HO_2 radicals.

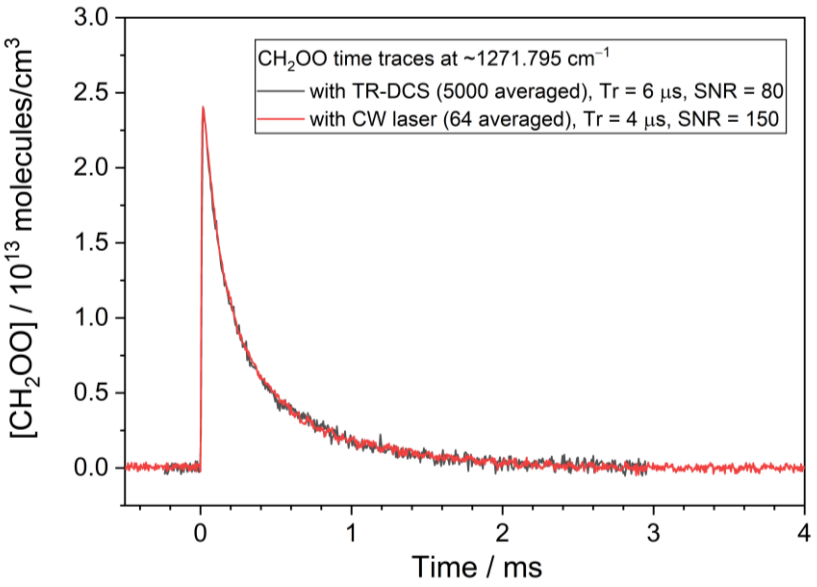

Figure S1. Comparison of the CH_2OO time traces recorded with different methods. The black trace measured by employing time-resolved dual-comb spectroscopy (TR-DCS) and the red trace measured by using the CW laser mode.

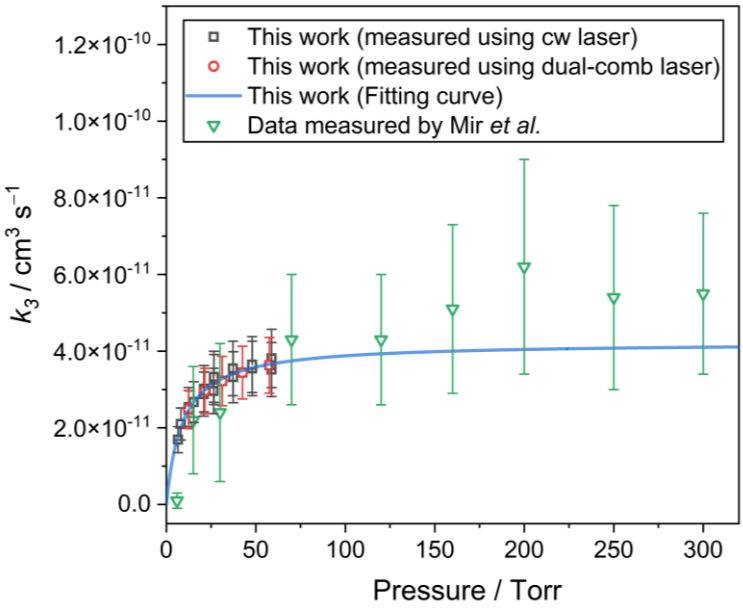

Figure S2. Rate coefficients for the CH_2OO + I reaction (k_3) as a function of the total pressure. The k_3 can be obtained by fitting the measured time traces of CH_2OO using the kinetic model (Table S1) with input of initial concentrations of CH_2I, I, and O_2, in which the rate coefficients at values listed in Table S1, except the k_3, were fixed while fitting the time traces. The blue curve derived by fitting the determined k_3 in this work with the Lindemann's equation, $k_3 = \{k_{3,0}\,[M] \times k_{3,\infty}\}/\{\,k_{3,0}\,[M] + k_{3,\infty}\}$. The rate coefficients in the low and high pressure limits, $k_{3,0}$ and $k_{3,\infty}$, are determined to be $(1.47\pm0.37)\times10^{-28}$ cm^6 molecule^{-1} s^{-1} and $(4.2\pm0.4)\times10^{-11}$ cm^3 molecule^{-1} s^{-1}, respectively. The data points shown by the green triangle are reported by Mir *et al.*[3]

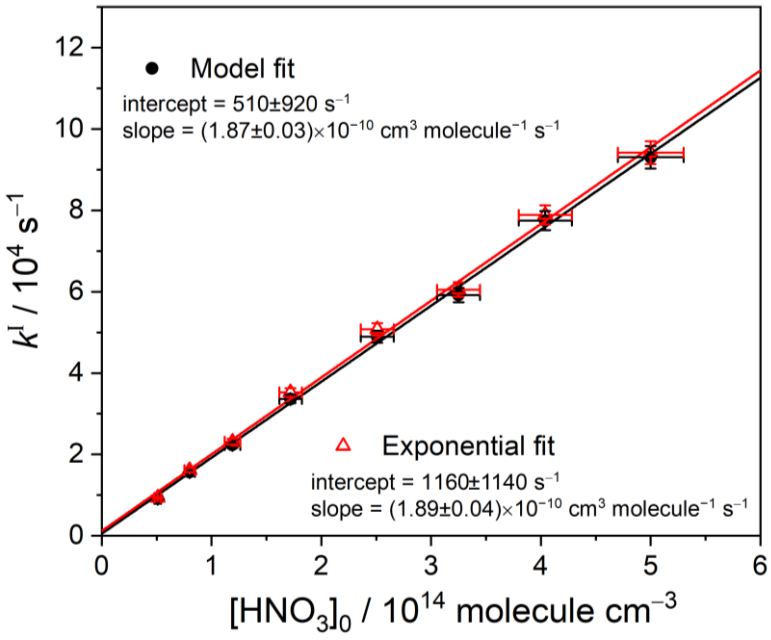

Figure S3. Comparison of plots of k^{I} vs. $[HNO_3]_0$ derived from model fit and single-exponential fit. The data correspond to experimental set 1 listed in Table S2.

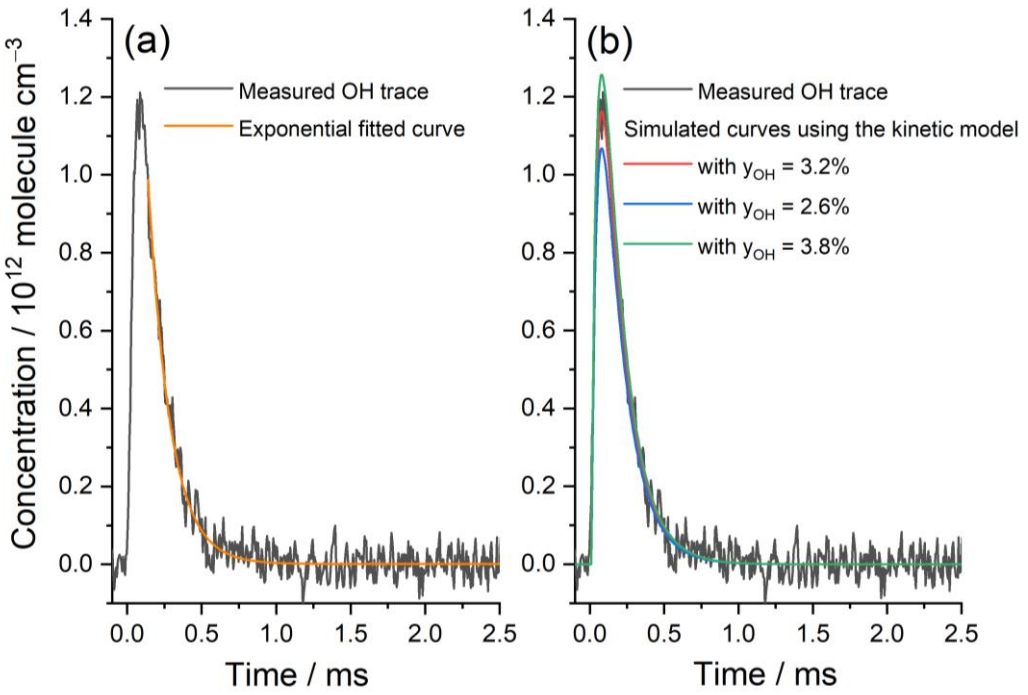

Figure S4. Comparison of the measured and simulated temporal profiles of the OH radical. (a) An overall decay rate (k_{18}) of 6800 s^{-1} was obtained by fitting the time trace with a single exponential-decay function. (b) A comparison of the measured and simulated temporal profiles with the fixed k_{18} of 6800 s^{-1} and the y_{OH} = 3.2%, 2.6%, and 3.8%. Here, the data correspond to the experiment 3 listed in Table S5.

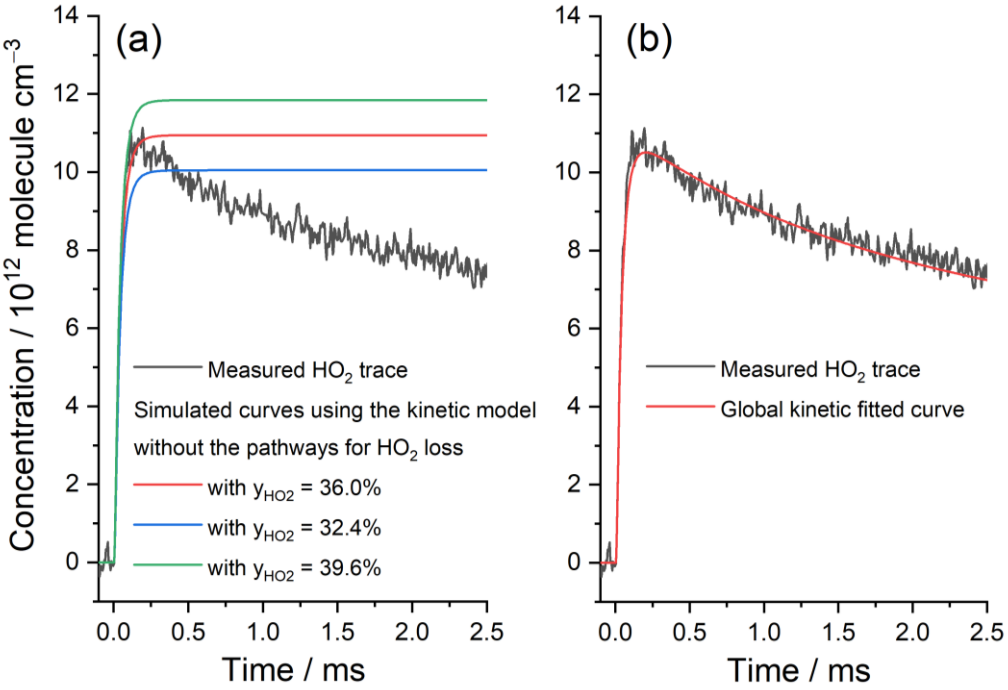

Figure S5. Comparison of the measured and simulated temporal profiles of the HO_2 radical. (a) A comparison of the measured and simulated temporal profiles excluding the loss pathways of HO_2 (R_{19}–R_{21}) and setting the y_{HO2} = 36.0%, 32.4%, and 39.6%. (b) A comparison of the measured and fitted curve with global kinetic model listed in Table S4 with the fixed y_{HO2} = 36.0%. Here, the data correspond to the experiment 3 listed in Table S5.

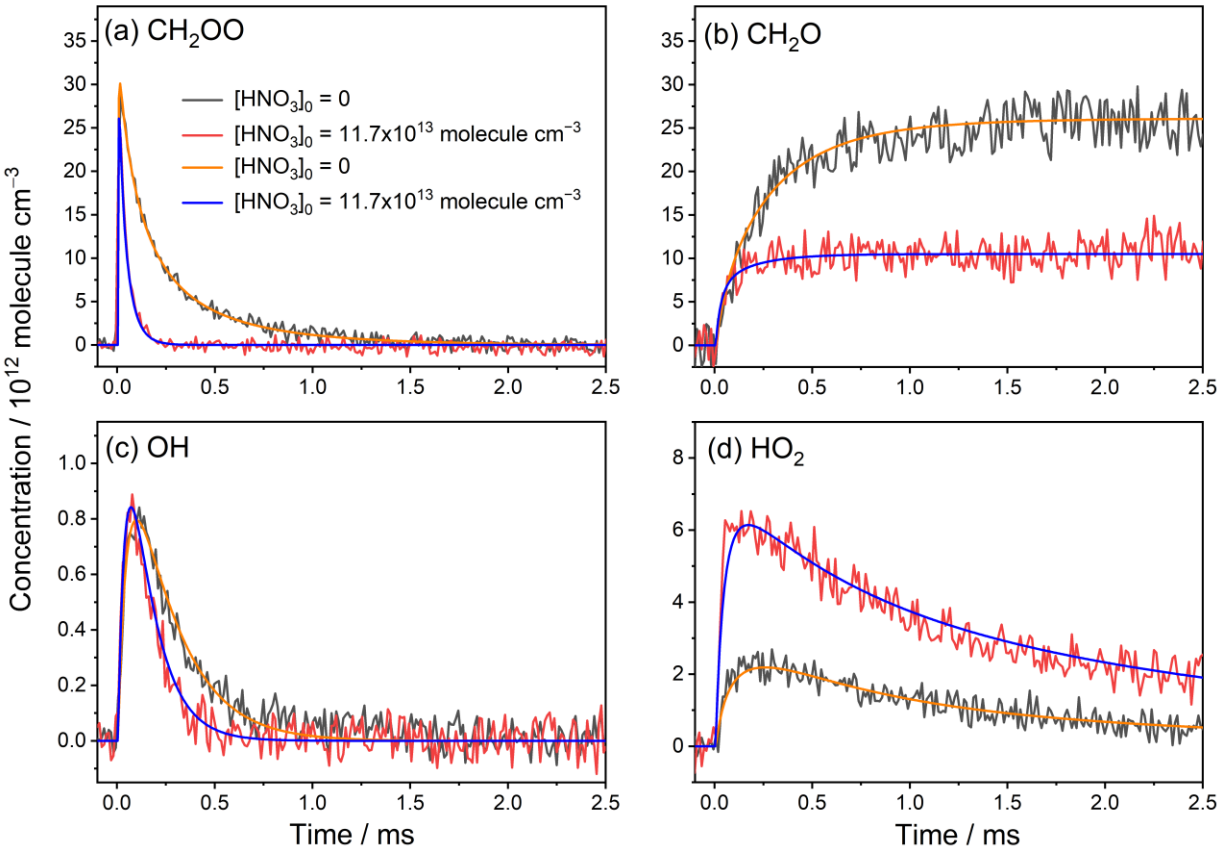

Figure S6. Comparison of temporal concentration profiles of (a) CH_2OO, (b) CH_2O, (c) OH, and (d) HO_2 with and without HNO_3 addition at 57.9 Torr. The temporal resolution of the measured temporal profiles (black and red) is 12 μs. The orange and blue curves represent the simulation profiles using the kinetic model shown in Table S4. Here, the data correspond to the experiments 4 and 5 listed in Table S5.

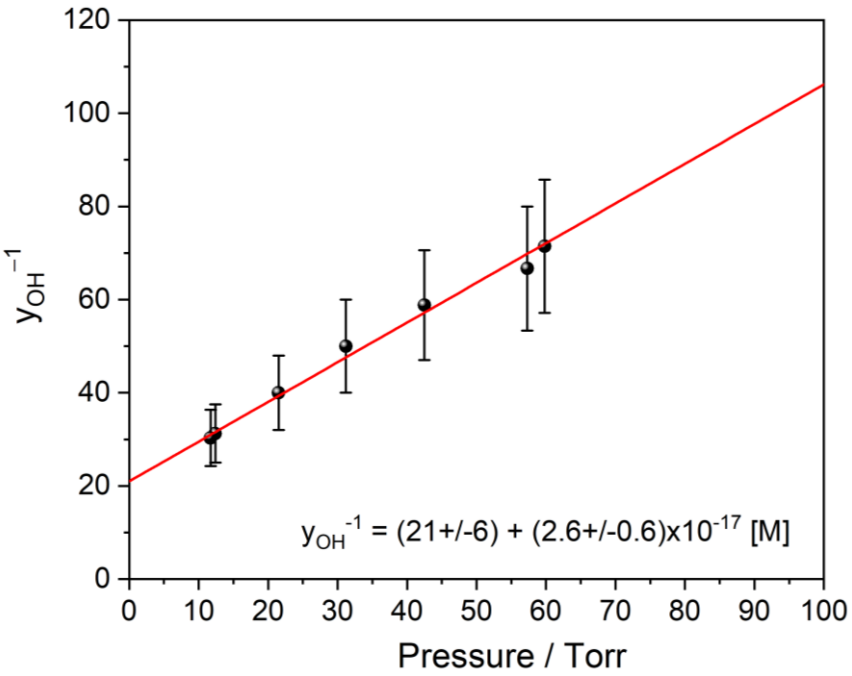

Figure S7. Inverse of the fractional yield of the OH + $CH_2(O)NO_3$ product channel (y_{OH}^{-1}) as a function of pressure. The red line indicates a linear fitting curve with an intercept of (21 ± 6) and a slope of (2.6±0.6) $\times 10^{-17}$ cm^3 $molecule^{-1}$.

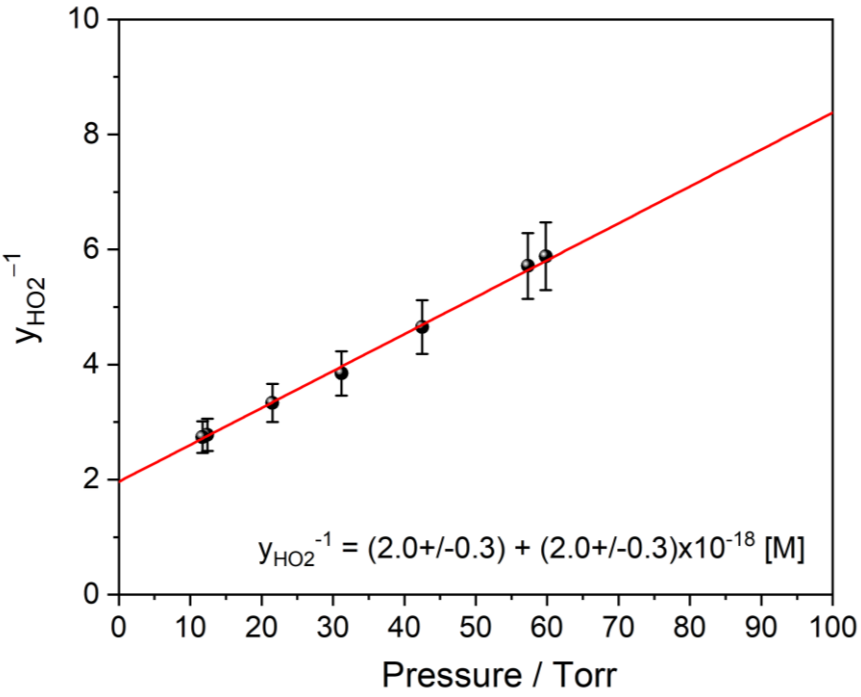

Figure S8. Inverse of the fractional yield of the NO_2 + CH_2O + HO_2 product channel (y_{HO2}^{-1}) as a function of pressure. The red line indicates a linear fitting curve with an intercept of (2.0 ± 0.3) and a slope of (2.0±0.3) ×10^{-18} cm^3 $molecule^{-1}$.

Table S1. The simplified model used for the kinetic study of the reaction $CH_2OO + HNO_3$.

	Reaction	Rate coefficient [a]	Ref.
R_{1a} [b]	$CH_2I + O_2 \rightarrow CH_2OO + I$	$\{1- 0.4/(1+1\times10^{-18}\ [M])\}\times1.7\times10^{-12}$ $/(1+1\times10^{-19}\ [M])$	1,2
R_{1b} [b]	$CH_2I + O_2 \xrightarrow{+M} ICH_2OO$	$1.7\times10^{-12} - 1.7\times10^{-12}/(1+1\times10^{-19}\ [M])$	1,2
R_{1c} [b]	$CH_2I + O_2 \rightarrow$ products	$1.7\times10^{-12} - (k_{1a} + k_{1b})$	1,2
R_2	$CH_2OO + CH_2OO \rightarrow 2CH_2O + O_2$	8.0×10^{-11}	3
R_3	$CH_2OO + I \xrightarrow{+M}$ product	$k_3 = \{1.47\times10^{-28}\ [M]\times4.2\times10^{-11}\}$ $/\{1.47\times10^{-28}\ [M]+4.2\times10^{-11}\}$	This work
R_4	$ICH_2OO + ICH_2OO \rightarrow 2ICH_2O + O_2$	9.0×10^{-11}	4
R_5	$ICH_2OO + I \rightarrow ICH_2O + IO$	3.5×10^{-11}	4
R_6	$IO + IO \rightarrow$ products	9.9×10^{-11}	5
R_7	$CH_2OO + HNO_3 \rightarrow$products	$k^I = k_7\times[HNO_3]_0$, fitted [c]	This work

[a] Rate coefficient in cm^3 $molecule^{-1}$ s^{-1}, [M] in molecule cm^{-3}.

[b] $k_{1a} + k_{1b} + k_{1c} = 1.7\times10^{-12}$ cm^3 $molecule^{-1}$ s^{-1}.

[c] k_7 represents the rate coefficients for the reaction $CH_2OO + HNO_3$, $k_{CH2OO+HNO3}$.

Table S2 Summary of experimental conditions and fitted rate coefficients k^{I}.

Set	Expt.	$[CH_2I]_0$ /10^{12} [c]	$[CH_2OO]_0$ /10^{12} [c]	$[O_2]$ /10^{17} [c]	P_T /Torr	$[HNO_3]_0$ [d] /10^{14} [c]	k^I [e] /10^4 s^{-1}
1 [a]	1	7.0	4.8	4.1	13.7	5.00	9.31
	2	7.0	4.8	4.1	13.7	4.04	7.75
	3	7.0	4.8	4.1	13.7	3.25	5.92
	4	7.0	4.8	4.1	13.7	2.51	4.89
	5	7.0	4.8	4.1	13.7	1.72	3.36
	6	7.0	4.8	4.1	13.7	1.19	2.23
	7	7.0	4.8	4.1	13.7	0.80	1.57
	8	7.0	4.8	4.1	13.7	0.51	0.91
2 [a]	9	4.5	3.0	2.6	8.7	3.27	6.48
	10	4.5	3.0	2.6	8.7	2.77	5.65
	11	4.5	3.0	2.6	8.7	2.20	4.11
	12	4.5	3.0	2.6	8.7	1.66	3.27
	13	4.5	3.0	2.6	8.7	1.27	2.48
	14	4.5	3.0	2.6	8.7	0.77	1.58
	15	4.5	3.0	2.6	8.7	0.49	0.94
3 [a]	16	7.1	4.8	3.4	12.2	3.73	7.16
	17	7.1	4.8	3.4	12.2	4.10	7.61
	18	7.1	4.8	3.4	12.2	2.50	4.65
	19	7.1	4.8	3.4	12.2	2.11	4.21
	20	7.1	4.8	3.4	12.2	1.41	2.57
	21	7.1	4.8	3.4	12.2	0.86	1.61
4 [a]	22	8.9	6.3	3.6	19.9	2.61	5.03
	23	8.9	6.3	3.6	19.9	2.15	4.00
	24	8.9	6.3	3.6	19.9	1.63	3.04
	25	8.9	6.3	3.6	19.9	1.11	2.30
	26	8.9	6.3	3.6	19.9	0.58	1.20
5 [a]	27	9.6	6.9	3.1	27.4	3.18	6.50
	28	9.6	6.9	3.1	27.4	2.62	5.22
	29	9.6	6.9	3.1	27.4	2.14	3.99
	30	9.6	6.9	3.1	27.4	1.76	3.28
	31	9.6	6.9	3.1	27.4	1.34	2.62
	32	9.6	6.9	3.1	27.4	0.92	1.85
6 [a]	33	11.2	8.2	3.4	36.9	3.24	6.48
	34	11.2	8.2	3.4	36.9	2.65	5.18
	35	11.2	8.2	3.4	36.9	2.20	4.34

	36	11.2	8.2	3.4	36.9	1.77	3.56
	37	11.2	8.2	3.4	36.9	1.34	2.90
7 [a]	38	6.5	4.6	3.6	58.6	3.32	6.29
	39	6.5	4.6	3.6	58.6	2.53	4.91
	40	6.5	4.6	3.6	58.6	1.75	3.27
	41	6.5	4.6	3.6	58.6	1.16	2.26
8 [a]	42	7.1	5.0	3.5	45.2	3.43	6.33
	43	7.1	5.0	3.5	45.2	2.49	4.73
	44	7.1	5.0	3.5	45.2	1.85	3.48
	45	7.1	5.0	3.5	45.2	1.33	2.75
	46	7.1	5.0	3.5	45.2	0.97	1.90
9 [a]	47	6.8	4.5	2.6	9.2	2.00	3.96
	48	6.8	4.5	2.6	9.2	2.70	5.28
	49	6.8	4.5	2.6	9.2	2.30	4.39
	50	6.8	4.5	2.6	9.2	1.57	2.95
	51	6.8	4.5	2.6	9.2	0.59	1.19
10 [b]	52	6.8	4.5	2.6	9.2	2.03	4.07
	53	6.8	4.5	2.6	9.2	2.51	4.61
	54	6.8	4.5	2.6	9.2	0.83	1.59
	55	6.8	4.5	2.6	9.2	1.21	2.26
11 [b]	56	10.8	7.1	1.6	6.3	2.32	4.32
	57	10.8	7.1	1.6	6.3	3.42	6.51
	58	10.8	7.1	1.6	6.3	4.49	8.62
	59	10.8	7.1	1.6	6.3	1.37	2.49
	60	10.8	7.1	1.6	6.3	0.92	1.71
	61	10.8	7.1	1.6	6.3	4.27	8.14
	62	10.8	7.1	1.6	6.3	2.96	5.50

[a] For the experiments, the CH_2OO line at 1271.795 cm^{-1} was probed.

[b] For the experiments, the CH_2OO line at 1237.622 cm^{-1} was probed.

[c] in unit of molecule cm^{-3}.

[d] The mixing ratio of the gaseous HNO_3 in the bath gas O_2/N_2 before injection into the reactor was determined using UV absorption spectra and the absorption cross section of HNO_3 in region 200–210 nm.[6] The $[HNO_3]_0$ in the reactor was estimated by the ratio of its flow rate to the total flow rate and the total pressure. Considering the errors of UV absorption cross section of HNO_3 at 200–210 nm (5 %), the flow rates (3 %), temperature (1 %), and pressure (1 %), an overall uncertainty of $[HNO_3]_0$ was estimated the to be 6 %.

[e] The k^1 obtained by fitting of CH_2OO traces with the kinetic model listed in Table S1.

Table S3 Summary of experimental and computational results for the $k_{CH2OO+HNO3}$.

Study	Temperature / T	Pressure / Torr	$[CH_2OO]_0$ $/10^{13}$ [a]	$[HNO_3]_0$ $/10^{13}$ [a]	$k_{CH2OO+HNO3}$ / 10^{-10} [b]
This work	296	6.3–58.6	0.30–0.82	4.9–50.0	1.9 ± 0.2
Foreman *et al*., 2016 [7]	295	27–35	1–2	8–23	5.4 ± 1.0
Chung *et al.*, 2022 [8]	298	40–70	>7	150–590	2.4 ± 0.4
Yang *et al.*, 2022 [9]	298	7.7–399.0	0.03–0.14	0.8–24.2	1.51 ± 0.45
Raghunath *et al*., 2017 [10]	295	20–760			5.1
Vereecken, 2017 [11]	250–350	760			2.5

[a] in unit of molecule cm^{-3}.

[b] in cm^3 $molecule^{-1}$ s^{-1}.

Table S4. Global kinetic model and rate coefficients employed for simulation of temporal profiles.

	Reaction	Rate coefficient [a]	Ref.
R_{1a} [c]	$CH_2I + O_2 \rightarrow CH_2OO + I$	$\{1- 0.4/(1+1\times10^{-18}\,[M])\}\times1.7\times10^{-12}$ $/(1+1\times10^{-19}\,[M])$	1,2
R_{1b} [c]	$CH_2I + O_2 \xrightarrow{+M} ICH_2OO$	$1.7\times10^{-12} - 1.7\times10^{-12}/(1+1\times10^{-19}\,[M])$	1,2
R_{1cI} [c]	$CH_2I + O_2 \rightarrow CH_2OO^{\#} + I$	1.2×10^{-13}	2
R_{1cII} [c]	$CH_2I + O_2 \rightarrow OH^{\#} + HCO^{\#} + I$	k_{1cII}	*d*
R_{1cIII} [c]	$CH_2I + O_2 \rightarrow 2H + CO_2 + I$	k_{1cIII}	*d*
R_{1cIV} [c]	$CH_2I + O_2 \rightarrow$ products + I	$1.7\times10^{-12} - (k_{1a} + k_{1b} + k_{1cI} + k_{1cII} + k_{1cIII})$	*d*
R_2	$CH_2OO + CH_2OO \rightarrow 2CH_2O + O_2$	8.0×10^{-11}	3
R_{3a}	$CH_2OO + I \xrightarrow{+M} CH_2O^{\#} + IO$	$0.56 \times k_3$	*d*
R_{3b}	$CH_2OO + I \xrightarrow{+M} ICH_2OO$	$0.44 \times k_3$	*d*
R_4	$ICH_2OO + ICH_2OO \rightarrow 2ICH_2O + O_2$	9.0×10^{-11}	4
R_5	$ICH_2OO + I \rightarrow ICH_2O + IO$	3.5×10^{-11}	4
R_6	$IO + IO \rightarrow$ products	9.9×10^{-11}	5
R_{7a}	$CH_2OO + HNO_3 \rightarrow OH + CH_2(O)NO_3$	$y_{OH} \times k_7$	*d*
R_{7b}	$CH_2OO + HNO_3 \rightarrow NO_2 + CH_2O + HO_2$	$y_{HO2} \times k_7$	*d*
R_{7c}	$CH_2OO + HNO_3 \rightarrow$ other products	$(1- y_{OH} - y_{HO2}) \times k_7$	*d*
R_8	$CH_2OO + CH_2OO^{\#} \rightarrow 2CH_2O^{\#} + O_2$	8.0×10^{-11}	2
R_9	$CH_2OO^{\#} + CH_2OO^{\#} \rightarrow 2CH_2O^{\#} + O_2$	8.0×10^{-11}	2
R_{10a}	$CH_2OO^{\#} + I \xrightarrow{+M} CH_2O^{\#} + IO$	set as same as k_{3a}	2
R_{10b}	$CH_2OO^{\#} + I \xrightarrow{+M} ICH_2OO$	set as same as k_{3b}	2
R_{11a}	$CH_2OO^{\#} + HNO_3 \rightarrow OH + CH_2(O)NO_3$	set as same as k_{7a}	*d*
R_{11b}	$CH_2OO^{\#} + HNO_3 \rightarrow NO_2 + CH_2O + HO_2$	set as same as k_{7b}	*d*
R_{11c}	$CH_2OO^{\#} + HNO_3 \rightarrow$ products	set as same as k_{7c}	*d*
R_{12a}	$CH_2OO^{\#} \rightarrow OH + HCO$	2000 [b]	2

R_{12b}	$CH_2OO^{\#} \rightarrow 2H + CO_2$	500 [b]	2
R_{12c}	$CH_2OO^{\#} \rightarrow$ products	200 [b]	2
R_{13}	$OH^{\#} \xrightarrow{+M} OH$	2.5×10^{4} [b]	12
R_{14}	$HCO^{\#} \xrightarrow{+M} HCO$	3.0×10^{4} [b]	13
R_{15}	$CH_2O^{\#} \xrightarrow{+M} CH_2O$	5000 [b]	2
R_{16}	$H + O_2 \xrightarrow{+M} HO_2$	7.0×10^{-14}	14
R_{17}	$HCO + O_2 \rightarrow HO_2 + CO$	5.5×10^{-12}	15
R_{18}	OH + others → products	k_{18} fitted [b]	*d*
R_{19}	$HO_2 + HO_2 \rightarrow H_2O_2 + O_2$	1.7×10^{-12}	16
R_{20}	$HO_2 + IO \rightarrow O_2 + HIO$	8.4×10^{-11}	5
R_{21}	HO_2 + others → products	k_{21} fitted [b]	*d*

[a] Rate coefficient in cm^3 $molecule^{-1}$ s^{-1}, unless specified, [M] in molecule cm^{-3}.

[b] Rate coefficient in s^{-1}.

[c] $k_{1a} + k_{1b} + k_{1cI} + k_{1cII} + k_{1cIII} + k_{1cIV} = 1.7\times10^{-12}$ cm^3 $molecule^{-1}$ s^{-1}.

[d] The values obtained in this work.

Table S5 Summary of experimental conditions, obtained rate coefficients, and branching ratios.

Expt.	$[CH_2I]_0$ /10^{13} [a]	$[HNO_3]_0$ /10^{13} [a]	$[O_2]$ /10^{17} [a]	P_T /Torr	k_{1cII} /10^{-14} [b]	k_{1cIII} /10^{-14} [b]	k_{18} /10^{3} [c]	k_{21} /10^{2} [c]	y_{OH} [d]	y_{HO2} [d]
1	3.8	0.0	2.0	12.5	4.0	1.8	5.3	2.6	–	–
2	3.8	7.2	2.0	12.5	4.0	1.8	6.8	0.5	0.032	0.360
3	3.8	14.7	2.0	12.5	4.0	1.8	6.8	0.5	0.032	0.360
4	4.5	0.0	2.3	57.9	3.0	1.4	6.2	2.6	–	–
5	4.5	11.7	2.3	57.9	3.0	1.4	8.0	2.5	0.015	0.175
6	4.3	0.0	1.8	21.5	3.8	1.7	5.4	2.6	–	–
7	4.3	9.6	1.8	21.5	3.8	1.7	6.9	1.0	0.025	0.300
8	4.3	0.0	2.0	31.2	3.5	1.6	5.6	2.6	–	–
9	4.3	9.4	2.0	31.2	3.5	1.6	7.2	1.6	0.020	0.260
10	4.5	0.0	2.1	42.5	3.3	1.5	5.8	2.6	–	–
12	4.5	8.9	2.1	42.5	3.3	1.5	7.5	2.2	0.017	0.215
13	3.0	0.0	1.9	11.7	4.0	1.8	5.3	2.6	–	–
14	3.0	9.1	1.9	11.7	4.0	1.8	6.8	0.5	0.033	0.365
15	3.0	5.4	1.9	11.7	4.0	1.8	6.8	0.5	0.033	0.365
16	3.0	0.0	2.3	59.8	3.0	1.4	6.2	2.6	–	–
17	3.0	6.5	2.3	59.8	3.0	1.4	8.0	2.5	0.014	0.170

[a] in unit of molecule cm^{-3}.

[b] in unit of cm^3 $molecule^{-1}$ s^{-1}.

[c] in unit of s^{-1}.

[d] The y_{OH} and y_{HO2} represent the branching ratios for the OH + $CH_2(O)NO_3$ and NO_2 + CH_2O + HO_2 product channels, respectively, in the CH_2OO + HNO_3 reaction.

References

(1) Ting, W.-L.; Chang, C.-H.; Lee, Y.-F.; Matsui, H.; Lee, Y.-P.; Lin, J. J.-M. Detailed mechanism of the $CH_2I + O_2$ reaction: Yield and self-reaction of the simplest Criegee intermediate CH_2OO. *The Journal of Chemical Physics* **2014,** *141,* 104308.

(2) Luo, P.-L.; Chen, I-Y. Synchronized two-color time-resolved dual-comb spectroscopy for quantitative detection of HO_x radicals formed from Criegee intermediates. *Anal. Chem.* **2022**, *94*, 5752–5759.

(3) Mir, Z. S.; Lewis, T. R.; Onel, L.; Blitz, M. A.; Seakins, P. W.; Stone, D. CH_2OO Criegee intermediate UV absorption cross-sections and kinetics of $CH_2OO + CH_2OO$ and $CH_2OO + I$ as a function of pressure. *Physical Chemistry Chemical Physics* **2020,** *22,* 9448–9459.

(4) Gravestock, T. J.; Blitz, M. A.; Bloss, W. J.; Heard, D. E. A multidimensional study of the reaction CH_2I+O_2: Products and atmospheric implications. *ChemPhysChem* **2010,** *11,* 3928–3941.

(5) Atkinson, R.; Baulch, D. L.; Cox, R. A.; Crowley, J. N.; Hampson, R. F.; Hynes, R. G.; Jenkin, M. E.; Rossi, M. J.; and Troe, J. Evaluated kinetic and photochemical data for atmospheric chemistry: Volume III – gas phase reactions of inorganic halogens. *Atmospheric Chemistry and Physics* **2007,** *7,* 981–1191.

(6) Sander, S. P.; Friedl, R. R.; Abbatt, J. P. D.; Barker, J. R.; Burkholder, J. B.; Golden, D. M.; Kolb, C. E.; Kurylo, M. J.; Moortgat, G. K.; Wine, P. H.; Huie, R. E.; Orkin, V. L. *Chemical Kinetics and Photochemical Data for Use in Atmospheric Studies;* Evaluation Number 17, JPL Publication 10-6; Jet Propulsion Laboratory: Pasadena, CA, 2011.

(7) Foreman, E. S.; Kapnas, K. M.; Murray, C. *Angew. Chem., Int. Ed.*, **2016**, *55*, 10419– 10422.

(8) Chung, C.-A.; Hsu, C.-W.; Lee, Y.-P. Infrared characterization of the products and rate coefficient of the reaction between Criegee Intermediate CH_2OO and HNO_3. *J. Phys. Chem. A* **2022**, *126*, 5738– 5750.

(9) Yang, J.-N.; Takahashi, K.; Lin, J.-M. Reaction kinetics of Criegee intermediates with nitric acid. *J. Phys. Chem. A* **2022**, *126*, 6160– 6170.

(10) Raghunath, P.; Lee, Y.-P.; Lin, M. C. Computational chemical kinetics for the reaction of Criegee intermediate CH_2OO with HNO_3 and its catalytic conversion to OH and HCO. *J. Phys. Chem. A* **2017**, *121*, 3871– 3878.

(11) Vereecken, L. The reaction of Criegee intermediates with acids and enols. *Phys. Chem. Chem. Phys.* **2017**, *19*, 28630– 28640.

(12) D'Ottone, L.; Bauer, D.; Campuzano-Jost, P.; Fardy, M.; Hynes, A. J. Vibrational deactivation studies of OH X $^2\Pi$ (v = 1–5) by N_2 and O_2. *Physical Chemistry Chemical Physics* **2004,** *6,* 4276–4282.

(13) Langford, A. O.; Moore, C. B. Reaction and relaxation of vibrationally excited formyl radicals. *The Journal of Chemical Physics* **1984,** *80,* 4204−4210.

(14) Michael, J. V.; Su, M.-C.; Sutherland, J. W.; Carroll, J. J.; Wagner, A. F. Rate constants for $H + O_2 + M \rightarrow HO_2 + M$ in seven bath gases. *The Journal of Physical Chemistry* **2002,** *106,* 5297–5313.

(15) Atkinson, R.; Baulch, D. L.; Cox, R. A.; Hampson, R. F.; Kerr, J. A.; Rossi, M. J.; Troe, J. Evaluated kinetic, photochemical and heterogeneous data for atmospheric chemistry: Supplement V. IUPAC Subcommittee on Gas Kinetic Data Evaluation for Atmospheric Chemistry. *Journal of Physical and Chemical*

Reference Data **1997,** *26,* 521−1011.

(16) Atkinson, R.; Baulch, D. L.; Cox, R. A.; Crowley, J. N.; Hampson, R. F.; Hynes, R. G.; Jenkin, M. E.; Rossi, M. J.; and Troe, J. Evaluated kinetic and photochemical data for atmospheric chemistry: Volume I – gas phase reactions of O_x, HO_x, NO_x and SO_x species. *Atmospheric Chemistry and Physics* **2004,** *4,* 1461–1738.